Journal of Alloys and Compounds 509 (2011) 5646–5654

Contents lists available at ScienceDirect

Journal of Alloys and Compounds

journal homepage: www.elsevier.com/locate/jallcom

Investigation on thermal and microstructural characterization of the TeO_2–WO_3 system

M. Çelikbilek*, A.E. Ersundu, N. Solak, S. Aydin*

Istanbul Technical University, Department of Metallurgical and Materials Engineering, Istanbul 34469, Turkey

ARTICLE INFO

Article history:
Received 11 January 2011
Received in revised form 17 February 2011
Accepted 19 February 2011
Available online 26 February 2011

Keywords:
TeO_2–WO_3
Phase equilibria
Glass forming range
Thermal analysis
Microstructural characterization

ABSTRACT

Thermal and microstructural characterization of the TeO_2–WO_3 binary system was accomplished by applying differential thermal analysis (DTA), X-ray diffraction (XRD) and scanning electron microscopy (SEM) techniques. Different compositions of the $(1-x)TeO_2$–xWO_3 system, where x varies between 0.02 and 0.80 in molar ratio were studied. The samples were prepared by melting high purity powder mixtures of TeO_2 and WO_3 in a platinum crucible with a closed lid at 750 °C for 30 min and quenching in water bath. The glass forming range of the binary system was detected as $0.04 \leq x \leq 0.35$ in molar ratio. As-cast samples were heat-treated above the crystallization peak temperatures at 550 °C for 24 h to obtain thermal stability and the phase stability of the binary system was investigated by performing systematical thermal, phase and microstructural characterizations with the heat-treated samples. The eutectic reaction of the binary system was detected at 617 ± 3 °C, the endothermic reaction indicating the phase transformation reaction of WO_3 from orthorhombic to tetragonal was determined at 743 ± 1 °C. α-TeO_2 and orthorhombic WO_3 crystalline phases were found to be present in the final structure when the total crystallization was achieved. Microstructural characterization of the TeO_2–WO_3 system was realized for a wide compositional range for the first time in the literature.

1. Introduction

Tellurite glasses have been investigated extensively due to their favorable physical and chemical properties such as, relatively low-phonon energy, high refractive index, high dielectric constant, good infrared transmissivity, low glass transition and melting temperature, thermal and chemical stability and high devitrification resistance [1–17]. Owing to these numerous properties, tellurite glasses have become preferable host materials for some infrared and infrared to visible upconversion applications in optical data storage, lasers, sensors and spectroscopic devices [5–8,11,14–20].

TeO_2 is the main but a conditional glass former; therefore, the addition of a secondary component such as heavy metal oxides, alkalis or halogens increases the glass forming ability [5–8]. The addition of WO_3 to tellurite glasses provides advantageous properties such as, doping in a wide range, modifying the composition by a third, fourth, and even fifth component, controlling the optical properties, enhancing the chemical stability and devitrification resistance of the glass [1,2,5]. In comparison to other tellurite glasses, tungsten-tellurite glasses have slightly higher phonon energy and higher glass transition temperature, therefore they can be used at high optical intensities without exposure to thermal damage [7,8,16,21].

Phase stability and phase equilibria of the popular TeO_2–WO_3 system need to be investigated in detail to develop and use tungsten-tellurite glasses in optical applications. A number of studies exist on optical properties of TeO_2–WO_3 binary system; however, limited studies are available on thermal stability, microstructural morphology, crystallization behavior and phase equilibria in the literature [1–5,22]. Blanchandin et al. [2] examined the phase stability of the system by realizing DSC and XRD analysis in a wide compositional range, improved the pseudo-binary phase diagram proposed by Safonov [19]. They also determined two new metastable crystalline phases, γ-TeO_2 and δ-TeO_2, which transform into stable α-TeO_2 (paratellurite) crystalline phase at higher temperatures. Öveçoğlu et al. [5] applied thermal and microstructural characterizations in the $(1-x)TeO_2$–xWO_3 system, for three compositions where $x = 0.15$, 0.25 and 0.30 in molar ratio using DTA, XRD and SEM techniques and determined the crystallization activation energy for $x = 0.15$ composition. Kosuge et al. [3] and Shaltout et al. [4] determined the glass transition, crystallization and melting temperatures for limited compositions by applying thermal analysis. Upender et al. [22] realized thermal and structural studies in the $(1-x)TeO_2$–xWO_3 system, where $0.10 \leq x \leq 0.40$ in molar ratio. However, the available data on thermal analysis in the

* Corresponding authors. Tel.: +90 212 285 6864; fax: +90 212 285 3427.
E-mail addresses: miraycelikbilek@gmail.com (M. Çelikbilek), saydin@itu.edu.tr (S. Aydin).

0925-8388/$ – see front matter © 2011 Elsevier B.V. All rights reserved.
doi:10.1016/j.jallcom.2011.02.109

literature show differences and apart from the SEM micrographs obtained by Öveçoğlu et al. [5] for $0.85TeO_2$–$0.15WO_3$ sample, no additional microstructural investigation was reported. Besides, according to the different sample preparation methods, several researchers determined different glass formation ranges for this binary system [1,2,4,9,20,21,23]. Also, there exist no information on the vitrification behavior of the tungsten-tellurite glasses.

As part of an ongoing research on tellurite based glasses in the TeO_2–WO_3–CdO system, the present study aims to investigate the glass forming range and phase equilibria of the fundamental TeO_2–WO_3 binary system by applying systematical thermal and phase characterizations in a wide compositional range. In this work, apart from obtaining the glass formation region and the phase equilibria of the binary system, which are almost in agreement with the literature, for the first time to our knowledge the numerical values of thermal measurement data were presented of the entire TeO_2–WO_3 system and microstructural characterization of the binary system was realized for a wide compositional range.

2. Experimental

In the experimental studies, 13 different samples of the $(1-x)TeO_2$–xWO_3 system, where x varies between 0.02 and 0.80 in molar ratio (now hereafter referred to as *TW2*–*TW80* samples, according to their WO_3 mol%), were prepared. All chemicals used in the experiments were reagent grade of TeO_2 (99.99% purity, Alfa Aesar Company) and WO_3 (99.8% purity, Alfa Aesar Company). Thoroughly mixed 5 g size powder batches were melted in a platinum crucible with a closed lid at 750 °C for 30 min and quenched in water bath. 750 °C was determined as the melting temperature by taking into account the binary phase diagram and the evaporation temperatures of the components.

The thermal characterization experiments were realized using differential thermal analysis (DTA) technique. DTA scans of the samples were carried out in a Perkin Elmer™ Diamond TG/DTA to determine the glass transition onset (T_g), crystallization onset and peak (T_c/T_p), eutectic onset and peak (T_e/T_m), liquidus onset and peak (T_{lo}/T_{lp}) and phase transformation onset and peak (T_{pto}/T_{pto}) temperatures. The temperature difference between the T_g and the first exothermic peak onset (T_c), $\Delta T = T_c - T_g$, indicating the glass stability and Hrubÿ parameter, $K_{gl} = (T_c - T_g)/(T_e - T_c)$, representing the glass forming tendency values were calculated. The glass transition onset temperatures (T_g) were determined as the inflection point of the endothermic change of the calorimetric signal. Onset temperatures were specified as the beginning of the reaction where the crystallization or melting first starts and peak temperatures represent the maximum value of the exotherm or endotherm. DTA scans were recorded using 25 mg of powdered samples. All thermal analysis was realized in a platinum crucible with a heating rate of 10 K/min under flowing (100 ml/min) argon gas. For each composition the DTA experiments were realized several times before the final temperature values were determined and the temperature precision was calculated as ±3 °C.

The density of the glass samples were determined at room temperature by a simple Archimedes's method using distilled water as an immersing liquid and a digital balance of sensitivity 10^{-4} g. The experimental data obtained by repeated measurements showed an error of ±0.2%.

According to the DTA results, as-cast samples were heat-treated above the crystallization peak temperatures at 550 °C for 24 h to obtain thermal stability of the system. X-ray diffraction (XRD) analyses were carried out on as-cast and heat-treated samples to confirm the amorphous character of the glassy samples and to determine the crystalline phases present in the final structure, respectively. The X-ray diffraction investigations were realized with powdered samples in a Bruker™ D8 Advanced Series powder diffractometer using Cu Kα radiation in the 2θ range from 10° to 90°. The Joint Committee on Powder Diffraction Standards (JCPDS) data files were used to determine the crystalline phases by comparing the reference patterns.

Scanning electron microscopy (SEM) investigations of the heat-treated samples were conducted with gold and platinum coated bulk samples in JEOL™ Model JSM 5410 and JEOL™ Model JSM 7000F microscopes linked with Noran 2100 Freedom and Oxford Inca energy dispersive X-ray spectrometer (EDS) attachments, respectively.

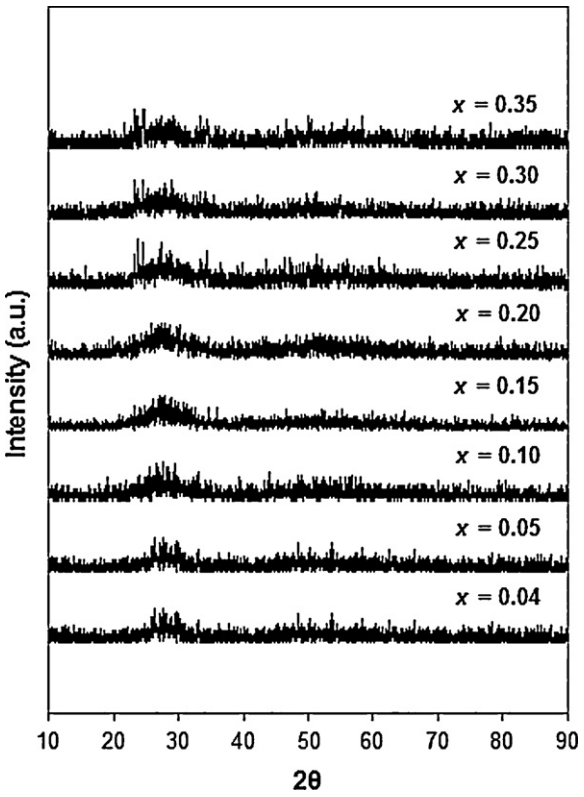

Fig. 1. XRD patterns of $(1-x)TeO_2$–xWO_3 glasses, where x varies between 0.04 and 0.35 in molar ratio.

3. Results and discussion

3.1. Characterization of the as-cast samples

In the present study, under the applied sample preparation conditions, as-cast samples with the compositions of $0.04 \leq x \leq 0.35$ in molar ratio in the $(1-x)TeO_2$–xWO_3 system were obtained as transparent and homogeneous glasses at macro size. Depending on the increasing WO_3 content, the glass samples showed a color change from yellowish to light brownish, representing a change in their optical properties.

XRD analyses were carried out with these as-cast samples in order to identify their glassy nature. As shown in Fig. 1, XRD patterns of the as-cast samples revealed no detectable peaks, proving the amorphous glassy structure.

There exist different results in the literature for the glass formation range of the TeO_2–WO_3 binary system depending on different sample preparation conditions; especially melting temperature and cooling technique of the melts (see Table 1). On the basis of the knowledge obtained from our earlier studies about the effect

Table 1
Glass forming region of the $(1-x)TeO_2$–xWO_3 system according to different sample preparation methods.

Research group	Glass forming region	Crucible material	Melting temperature	Cooling condition
Blanchandin et al. [2]	$0.10 \leq x \leq 0.30$	Platinum	850 °C	Casting onto a brass mold at 60 °C
Shaltout et al. [4]	$0.05 \leq x \leq 0.50$	Platinum	800–1000 °C	Casting onto a stainless steel mold at 25 °C
Charton et al. [9]	$x \leq 0.325$	Platinum	900 °C	Quenched in ice bath at −10 °C
Yakhkind et al. [20]	$0.11 \leq x \leq 0.33$	Gold	700–1000 °C	Casting onto a metal mold at 25 °C
Kozhukharov et al. [21]	$0.11 \leq x \leq 0.33$	Quartz	800–1000 °C	Casting on a copper plate at 25 °C
Al-Ani et al. [23]	$x \leq 0.33$	Alumina	800–950 °C	Blowing molten glass using an alumina tube with a fine bore

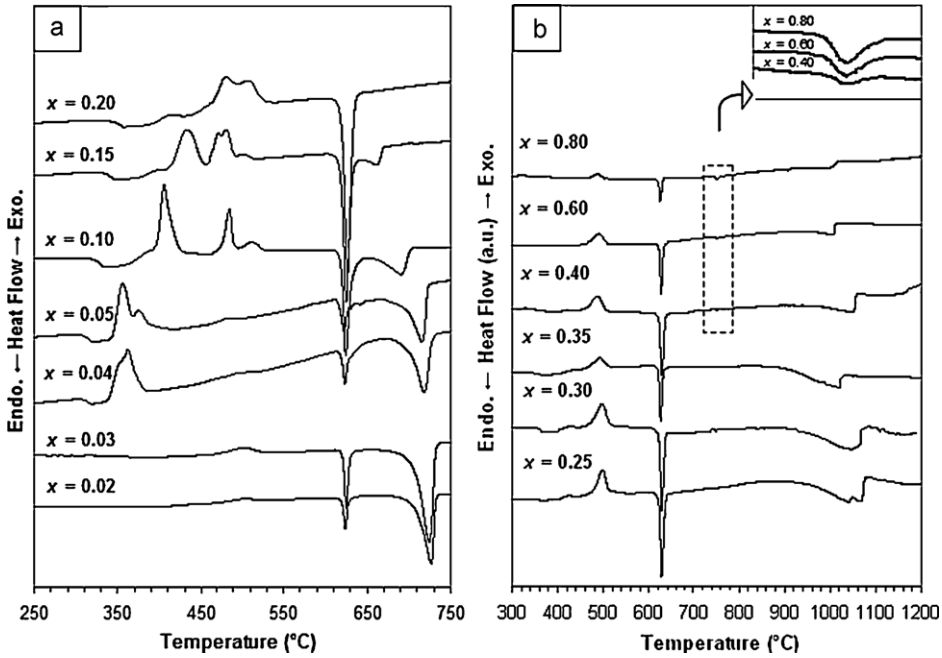

Fig. 2. DTA curves of as-cast samples of $(1-x)TeO_2$–xWO_3, (a) where x varies between 0.02 and 0.20, (b) where x varies between 0.25 and 0.80, in molar ratio.

of different cooling conditions on the glass forming ability of the TeO_2–WO_3 binary system, it is known that high melting temperatures may extend the glass stability region and elevate the glass forming tendency. Besides, in our earlier study we found that the glass stability and the glass forming tendency of the samples quenched in ice bath is higher than the glasses prepared by quenching in water bath or casting onto a mold [24]. The glass forming range determined in this study is in agreement with the reported intervals in the literature. However, comparing with the glass formation ranges reported in the literature (see Table 1) the glass forming region determined in this study is considerably wider despite the lower melting temperature and the applied cooling technique.

DTA analyses were carried out to determine the thermal behavior of the simple eutectic-type TeO_2–WO_3 binary system [2,5]. DTA thermograms of the hypoeutectic as-cast samples ($0.02 \leq x \leq 0.20$) in the temperature range of 250–750 °C and hypereutectic as-cast samples ($0.25 \leq x \leq 0.80$) in the temperature range of 300–1200 °C are presented in Fig. 2 and the thermal analysis details are given in Table 2. For the glass samples, a broad endothermic change of the calorimetric signal corresponding to the glass transition was observed between 308 and 353 °C. The detected glass transition values (T_g) are lower than the existing values in the literature [3–5,22]. The glass transition temperatures shifted to higher values with the increasing WO_3 content as reported in the literature [2,4,5,22].

As can be seen in Fig. 3a, the glass transition and the crystallization onset temperatures shifted to higher values with the increasing WO_3 content and after a certain composition ($x = 0.25$), the T_g and T_c values showed a slight decrease, which is also stated in the literature [2,4,5,24]. The glass stability parameter was calculated for all glass samples and as listed in Table 2 in detail, ΔT values of the samples increased with the increasing WO_3 content (see Fig. 3b), reached a maximum of 124 °C for *TW*25 sample and then showed a slight decrease. The glass stability provides a good estimate of glass crystallization tendency. With a different approach, El-Mallawany et al. [25] calculated the thermal stability of the glass samples by subtracting the glass transition onset temperature from the first exothermic peak temperature and reported that the glass stability should usually be larger than 100 °C to obtain thick glass samples for optical applications. Taking into account El-Mallawany et al.'s

Table 2
Values of glass transition onset (T_g), crystallization onset and peak (T_c/T_p), eutectic onset and peak (T_e/T_m), liquidus onset and peak (T_{lo}/T_{lp}), phase transformation onset and peak (T_{pto}/T_{ptp}), glass stability (ΔT), glass forming tendency (K_{gl}) of the as-cast samples, with an error estimate of ±3 °C.

Compositions (mol%)		T_g (°C)	T_{c1}/T_{p1} (°C)	T_{c2}/T_{p2} (°C)	T_{c3}/T_{p3} (°C)	T_{c4}/T_{p4} (°C)	T_e/T_m (°C)	T_{lo}/T_{lp} (°C)	T_{pt} (°C)	ΔT	K_{gl}
TeO_2	WO_3										
98	2		480/504				619/623	711/725			
97	3		473/506				619/623	705/722			
96	4	308	340/–	–/362	–/494		618/623	–/718		32	0,12
95	5	309	345/356	–/375	–/482		618/623	641/715		36	0,13
90	10	321	363/–	–/405	476/485	–/512	619/623	–/689		42	0,16
85	15	335	414/433	–/471	–/481	–/502	618/626	–/658		79	0,39
80	20	344	439/–	–/481	–/508		620/627			95	0,53
75	25	352	476/498				618/623	761/830		124	0,87
70	30	353	475/496				621/627			122	0,84
65	35	350	468/493				620/627			118	0,75
60	40		458/485				620/625		743/747		
40	60		467/490				619/624		743/747		
20	80		466/489				617/622		743/747		

–: Undetermined values.

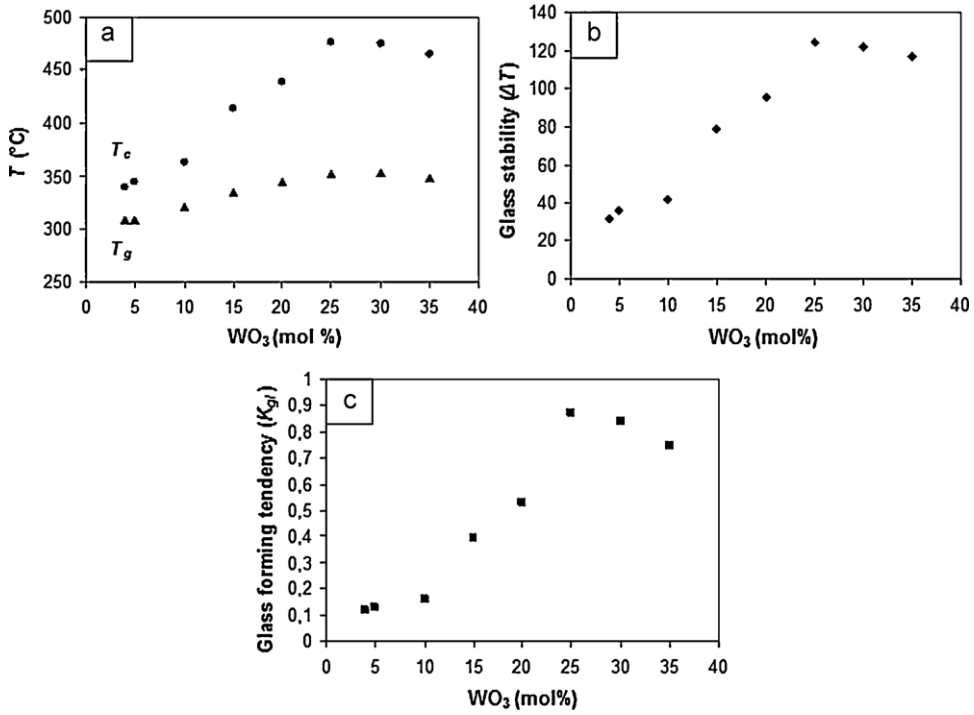

Fig. 3. (a) Glass transition temperature, T_g, crystallization onset temperature, T_c, (b) glass stability, ΔT, (c) glass forming tendency, K_{gl}, values of $(1-x)TeO_2$–xWO_3 glasses.

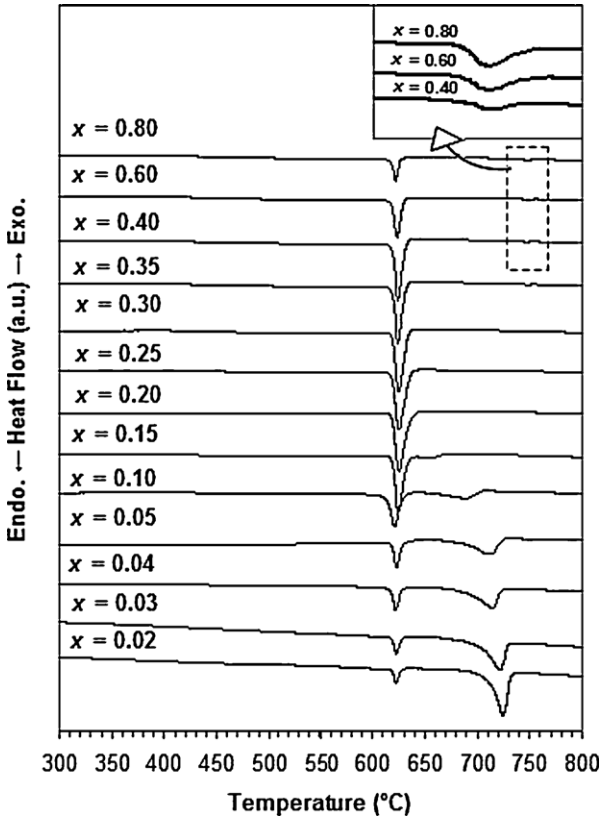

Fig. 4. DTA curves of heat-treated samples of $(1-x)TeO_2$–xWO_3, where x varies between 0.02 and 0.80 in molar ratio.

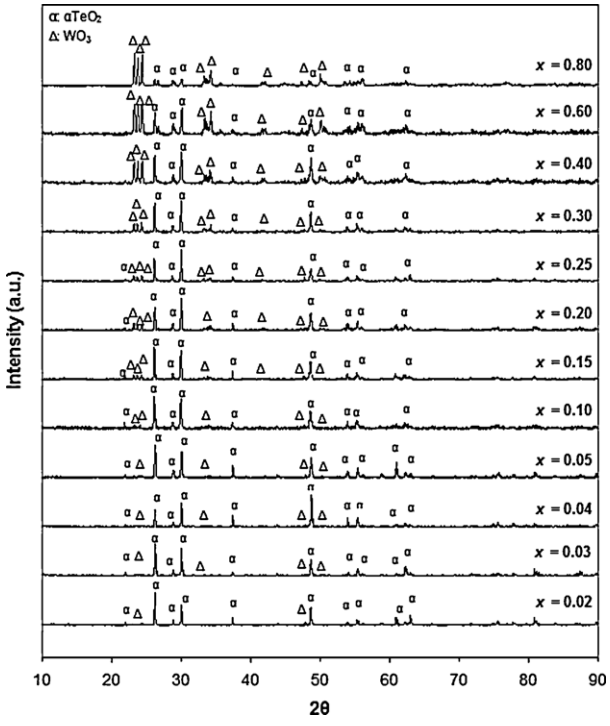

Fig. 5. XRD patterns of $(1-x)TeO_2$–xWO_3 samples heat treated at 550 °C for 24 h, where x varies between 0.02 and 0.80 in molar ratio.

[25] approach; it can be concluded that ΔT values obtained in the present study for glasses where $x \geq 0.25$ in molar ratio are adequate to obtain thick glasses. The glass forming tendency parameter, which is also named as Hrubÿ parameter in the literature [26] was also calculated for all glass samples and the K_{gl} values were found to be proportional to the glass stability (see Fig. 3c). Using the Hrubÿ parameter, *TW*25 sample was found to be the most stable glass, while the glass forming tendency of *TW*4 sample was determined as the lowest. By taking into account the glass stability value and Hrubÿ parameter *TW*25 glass showed the highest vitrification behavior. As reported in the previous structural studies on tungsten-tellurite glasses, T_g, T_c, ΔT, K_{gl} values, which represent

the vitrification behavior of glasses, showed an increase with the increasing WO_3 content since the addition of WO_3 promotes the formation of TeO_3/TeO_{3+1} units and WO_6 units in tungsten-tellurite glasses at the exposure of TeO_4 and WO_4 units [4,16,17,22,27,28].

As can be seen from Table 2 and Fig. 2, number of exothermic reactions observed in the DTA thermograms varies with the composition. The reason of several crystallization steps observed in the DTA thermograms was due to the polymorphic nature of TeO_2 at elevated temperatures. However, in the present study the number of crystallization reactions decreased by increasing WO_3 content and only one exothermic peak was observed for compositions where $x \geq 0.20$ in molar ratio. The crystallization reaction results observed in the present study show consistency with the data obtained by Blanchandin et al. [2], while different number of crystallization reactions were reported in the literature by several research groups [3–5,22].

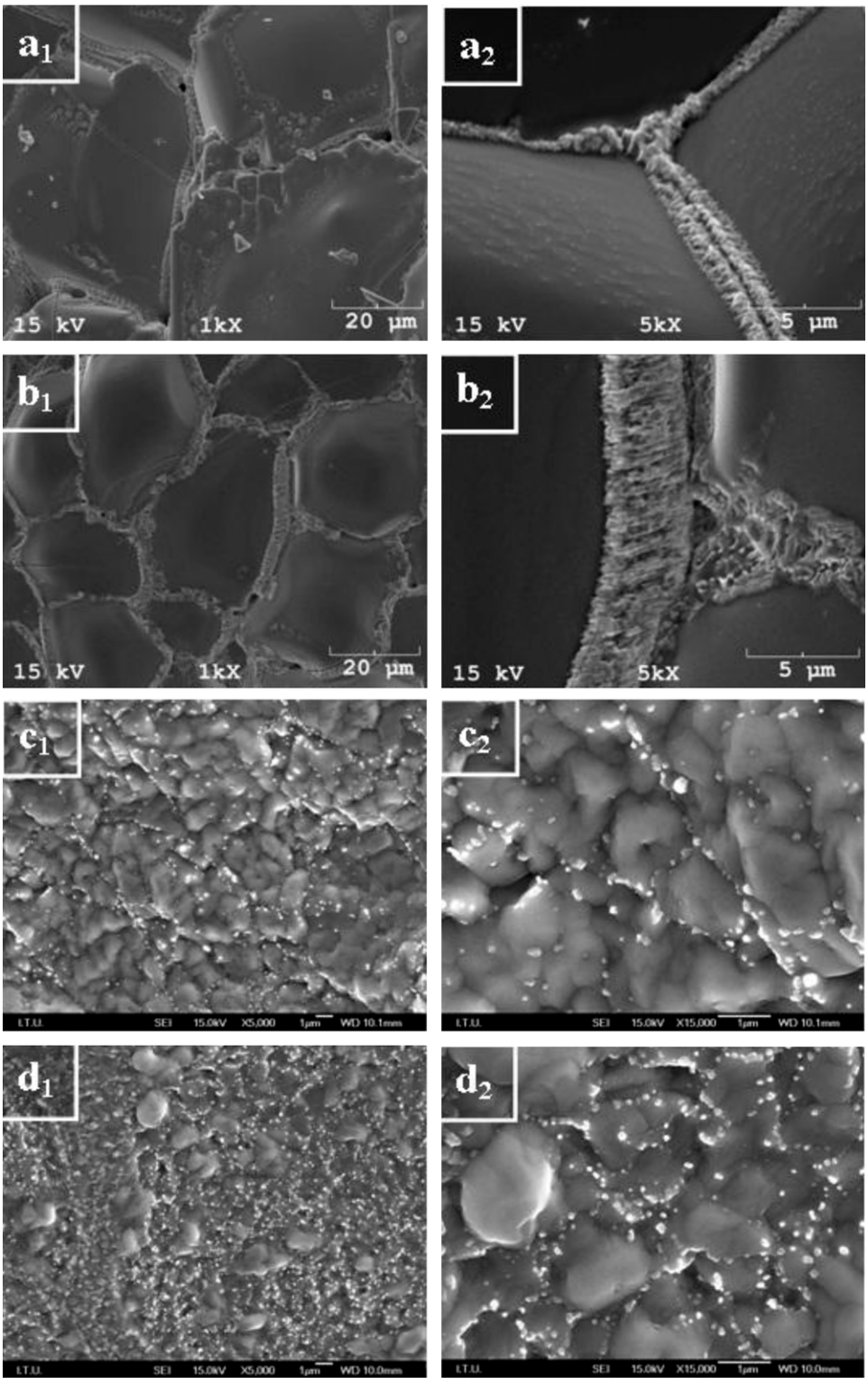

Fig. 6. SEM micrographs of the $(1-x)TeO_2$–xWO_3 samples heat-treated at 550 °C, with high and low magnifications, where $x = (a_1–a_2)$ 0.02, $(b_1–b_2)$ 0.03, $(c_1–c_2)$ 0.04, $(d_1–d_2)$ 0.05, $(e_1–e_2)$ 0.10, $(f_1–f_2)$ 0.15, $(g_1–g_2)$ 0.20, $(h_1–h_2)$ 0.25, $(i_1–i_2)$ 0.30, $(j_1–j_2)$ 0.35, $(k_1–k_2)$ 0.40, $(l_1–l_2)$ 0.60, $(m_1–m_2)$ 0.80, in molar ratio.

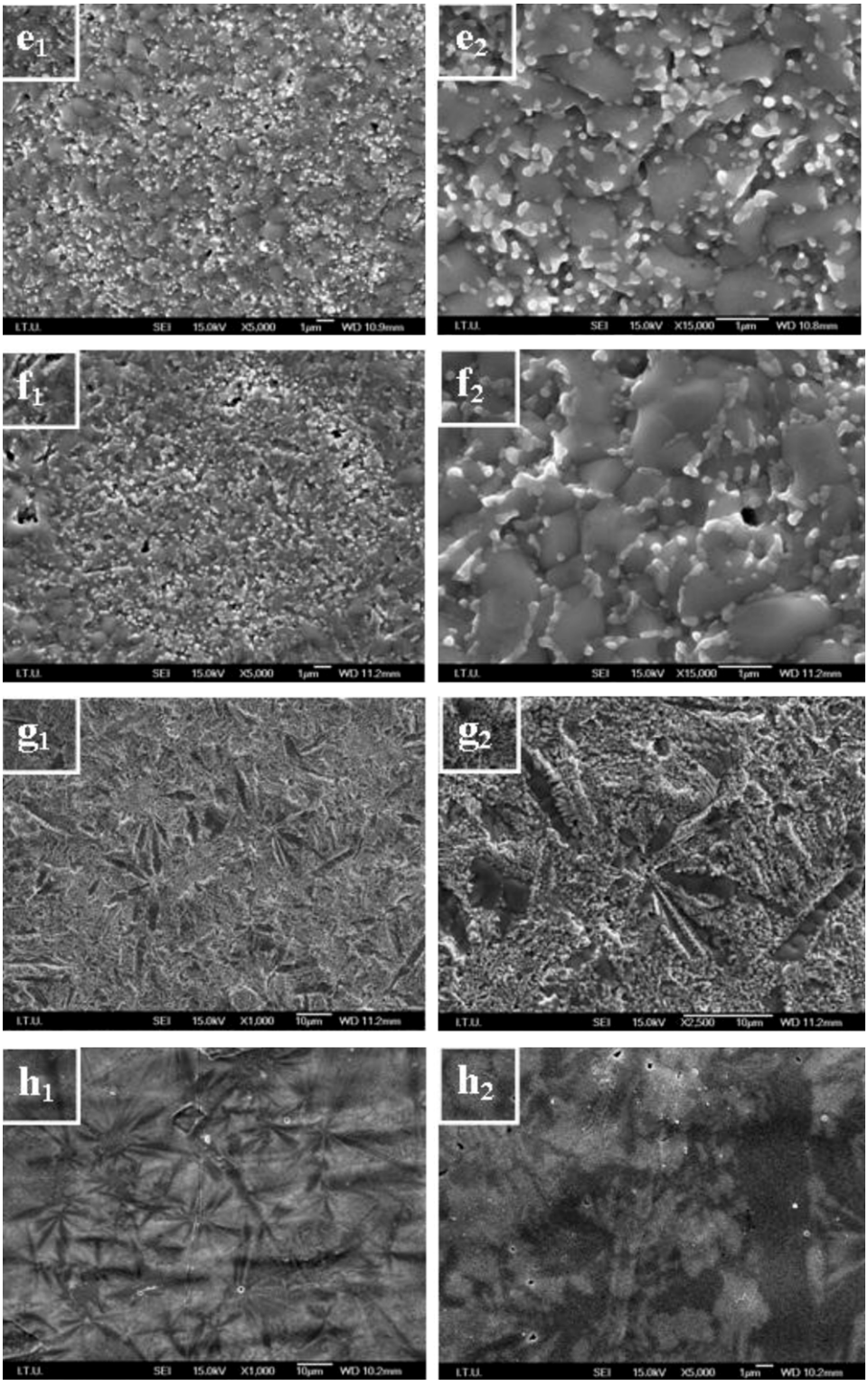

Fig. 6. (*Continued*)

According to the DTA results obtained over a wide range of compositions, all the samples exhibited a similar endothermic peak, indicating the eutectic reaction of the TeO_2–WO_3 binary system. Onset and peak temperatures of the eutectic reaction were determined as $619 \pm 2\,^{\circ}C$ and $625 \pm 3\,^{\circ}C$, respectively (see Fig. 2 and Table 2). The eutectic reaction of the TeO_2–WO_3 system temperature was also detected approximately at the similar values by three different research groups in the literature [2,5,19].

In the hypo-eutectic region, for the samples containing less than 20 mol% WO_3, second endothermic peaks representing the liquidus reaction were determined. With the increasing WO_3 content, the liquidus temperatures approached to the eutectic temperatures and disappeared at around the eutectic composition. The liquidus reaction was also determined in the hyper-eutectic region of the binary system for *TW*25 sample at 761 °C. Due to the possible evaporation of TeO_2 at temperatures higher than 900 °C [2], the

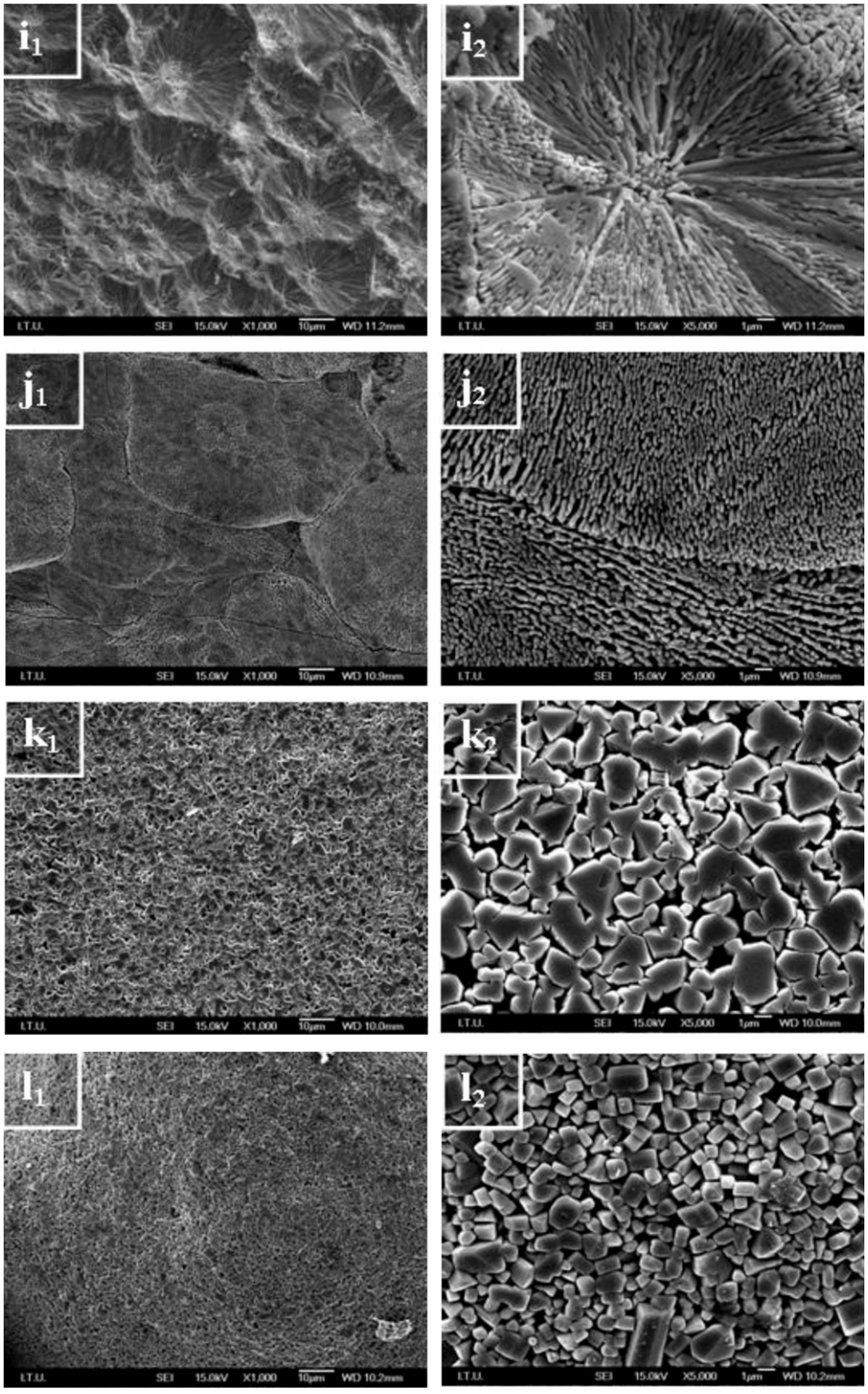

Fig. 6. (*Continued*)

liquidus reaction temperatures could not be determined for samples containing more than 25 mol% of WO_3. The endothermic peaks situated around 950 °C on DTA thermograms in Fig. 2b represent the possible TeO_2 evaporation which was also observed by the thermogravimetric signals.

For samples where $x \geq 0.40$, secondary weak endothermic peaks were determined at 743 ± 1 °C (see Fig. 2b inset) representing the phase transformation from orthorhombic to tetragonal WO_3, which was also reported in the literature at 740 °C [29]. Despite repeated experiments for $x < 0.40$ samples, the second endothermic peak corresponding to the phase transformation reaction could not be detected possibly due to the less amount of WO_3 content.

The density of the glass samples regularly increase from 5.29 to 6.24 g/cm^3 with the increasing WO_3 content. The calculated density

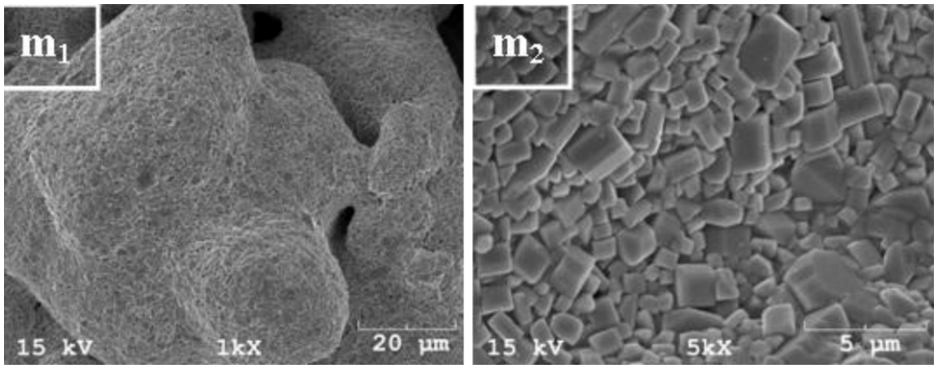

Fig. 6. (*Continued*).

values of the samples with high WO_3 content are in good agreement with the previously reported data [2,20,25], however, for the samples containing small amount of WO_3, calculated density values are lower than the literature values except those found by Al-Ani et al. [23].

3.2. Characterization of the heat-treated samples

As-cast samples were heat-treated above the all crystallization peak temperatures at 550 °C in order to obtain thermal equilibrium (see Fig. 2). According to the DTA results of the heat-treated samples shown in Fig. 4, no crystallization reaction was detected for the whole composition range. As shown in Fig. 4, for $x \leq 0.20$ compositions, two endothermic peaks were determined corresponding to the eutectic and liquidus reactions. The increase in the WO_3 content leads to the approach of liquidus peak to the eutectic temperature. An endothermic peak, indicating the eutectic reaction of the TeO_2–WO_3 binary system was determined at 617 ± 3 °C. For compositions above 40 mol% WO_3, secondary weak endothermic peaks representing the phase transformation from orthorhombic to tetragonal WO_3 were determined at 743 ± 1 °C (see Fig. 4 inset). Endothermic peaks corresponding to the eutectic, liquidus and phase transformation reactions obtained for the as-cast and heat-treated samples were detected almost at the same temperature values.

In the literature, eutectic reaction of the TeO_2–WO_3 binary system was reported as 630 °C for 16.3 mol% by Safonov et al. [19]. Later on, Blanchandin et al. [2] determined the eutectic temperature at 622 ± 5 °C and the eutectic composition at 22 ± 1 mol% WO_3 by DSC studies. The eutectic temperature was recently confirmed by Öveçoğlu et al. [5], as 622 °C. Degeneration of the eutectic temperature reported by Blanchandin et al. [2] for low WO_3 contents (where x varies between 0.00 and 0.10, in molar ratio) was not observed in the present study. At hypo-eutectic region of the phase diagram, numerous experiments were realized and the same eutectic onset temperature interval was determined for all attempts.

XRD analyses were carried out on heat-treated samples at 550 °C to identify crystalline phases present in the final structure. XRD patterns of the fully crystalline samples are given in Fig. 5. As it can be seen from Fig. 5, when the crystallization was fully achieved, the XRD patterns of the heat treated samples matched with paratellurite (α-TeO_2), which has a tetragonal crystal structure with the calculated lattice parameters $a = 0.478$ nm and $c = 0.760$ nm (space group: $P41212$) and orthorhombic WO_3, with the lattice parameters $a = 0.726$ nm, $b = 0.749$ nm and $c = 0.765$ nm (space group: $P12/n$). The calculated lattice parameters were found to be almost the same with the reference card files [30,31]. With the increasing WO_3 content, α-TeO_2 peak intensities showed a decrease, while orthorhombic WO_3 became more pronounced in the structure.

SEM investigations were performed on the heat-treated samples in order to identify the morphology of the final microstructures when the crystallization was completed. Thusly, microstructural morphology of the TeO_2–WO_3 system was detected for the first time in the literature for the entire system. Fig. 6 represents the SEM micrographs of $(1-x)TeO_2$–xWO_3 samples for different magnifications.

Fig. 6a_1–a_2 and b_1–b_2 are the representative SEM micrographs of the *TW2* and *TW3* samples with the magnifications of ×1000 and ×5000 revealing the presence of grain like crystallites (40–80 μm size) in the general structure with a secondary phase precipitated along the grain boundaries. EDS spectra taken from the grains and the grain boundaries showed that the WO_3 content is four times higher along the grain boundaries than the grains for these compositions.

A strong decrease in the size of the grains (1–1.5 μm size) were detected with the presence of a precipitated secondary phase along the grain boundaries in the SEM micrographs of samples containing 4–15 mol% WO_3 with the magnifications of X5000 and X15.000 (Fig. 6c_1–c_2 to f_1–f_2). According to the SEM photos, almost no difference was detected for the microstuctural morphology of the *TW*4, *TW*5, *TW*10 and *TW*15 samples apart from the dimensional change in the grain size.

SEM micrographs of *TW*20, *TW*25 and *TW*30 samples (Fig. 6g_1–g_2 to i_1–i_2) generally showed the degradation of grains and the formation of centrosymmetric leaf-like crystallites which show dendritic rod-like structure with various orientations at higher magnifications. Similar lamellar crystals in shape of long rods oriented in various directions have been observed in the literature by Öveçoğlu et al. [5] for $0.85TeO_2$–$0.15WO_3$ composition.

Fig. 6j_1–j_2 are the representative SEM micrographs of the *TW*35 sample. The degradation of the centro-symmetric leaf like structures and the regeneration of the grains were detected. Rod-like crystallites along the grains constituted the general matrix.

SEM micrographs of *TW*40 sample are shown in Fig. 6k_1–k_2. Small polygonal crystallites existed along the whole structure, approximately ranging between 2 and 4 μm in size.

For *TW*60 and *TW*80 samples, SEM micrographs are given in Fig. 6l_1–l_2 and m_1–m_2 revealing small grains along the whole structure, having crystal sizes about 0.5–2 μm.

In general the SEM micrographs of $(1-x)TeO_2$–xWO_3 samples heat-treated at 550 °C revealed the presence of α-TeO_2 primary grains and the formation of WO_3 crystallites in accordance with the increasing WO_3 content. It was observed that with increasing WO_3 content, the granular shape of the α-TeO_2 crystalline phase converted into a leaf like structure, as also reported in the literature [5]. Likewise, the precipitated WO_3 crystalline phase along the grain boundaries turned into angular grains and spread throughout the structure with increasing WO_3 content.

4. Conclusions

Thermal and microstructural investigations were conducted in the binary TeO_2– WO_3 system, with 13 different compositions of $(1-x)TeO_2$–xWO_3 (where $x = 0.02$–0.80 in molar ratio), using DTA, XRD and SEM techniques. The glass forming region of the binary system was determined as $0.04 \leq x \leq 0.35$ and the glass sample containing 25 mol% WO_3 showed the highest vitrification behavior. A binary eutectic: liquid $\rightarrow$ α-TeO_2 + WO_3 was detected at $619 \pm 2\,^{\circ}C$ for the as-cast samples. At $743 \pm 1\,^{\circ}C$, a phase transformation from orthorhombic to tetragonal WO_3 was determined. In order to obtain thermal stability, as-cast samples were heat-treated above the crystallization peak temperatures at $550\,^{\circ}C$ for 24 h. Endothermic peaks detected with the heat-treated samples indicating the eutectic ($617 \pm 3\,^{\circ}C$) and phase transformation ($743 \pm 1\,^{\circ}C$) reactions confirmed the temperature values obtained with the as-cast samples. Based on the determined XRD and SEM investigations, α-TeO_2 and orthorhombic WO_3 crystalline phases were found when the final crystallization was achieved. SEM micrographs revealed the conversion of granular shape α-TeO_2 crystalline phase into a leaf like structure and the change of the precipitated WO_3 crystalline phase along the grain boundaries into angular grains with the increasing WO_3 content. Although similar thermal stability results were obtained with the literature, in the present study numerical values of the thermal measurement data of the TeO_2–WO_3 system were presented for a wide compositional range and microstructural study of the entire TeO_2–WO_3 system was realized for the first time to our knowledge in the literature.

Acknowledgement

The authors wish to express their thanks to The Scientific & Technological Research Council of Turkey (TUBITAK) for the financial support under the project numbered 108M077.

References

[1] R.A.H. El-Mallawany, Tellurite Glasses Handbook, CRC Press, Boca Raton/London/New York/Washington, DC, 2002.
[2] S. Blanchandin, P. Marchet, P. Thomas, J.C. Champarnaud-Mesjard, B. Frit, A. Chagraoui, J. Mater. Sci. 34 (1999) 4285–4292.
[3] T. Kosuge, Y. Benino, V. Dimitrov, R. Sato, T. Komatsu, J. Non-Cryst. Solids 242 (1998) 154–164.
[4] I. Shaltout, Y. Tang, R. Braunstein, A.M. Abu-Elazm, J. Phys. Chem. Solids 56 (1994) 141–150.
[5] M.L. Öveçoğlu, G. Özen, S. Cenk, J. Eur. Ceram. Soc. 26 (2006) 1149–1158.
[6] A.E. Ersundu, G. Karaduman, M. Çelikbilek, N. Solak, S. Aydin, J. Eur. Ceram. Soc. 30 (2010) 3087–3092.
[7] A.E. Ersundu, G. Karaduman, M. Çelikbilek, N. Solak, S. Aydin, J. Alloys Compd. 508 (2010) 266–272.
[8] M. Çelikbilek, A.E. Ersundu, N. Solak, S. Aydin, J. Non-Cryst. Solids 357 (2011) 88–95.
[9] P. Charton, L. Gengembre, P. Armand, J. Solid State Chem. 168 (2002) 175–183.
[10] D. Lezal, J. Pedlikova, P. Kostka, J. Bludska, M. Poulain, J. Zavadil, J. Non-Cryst. Solids 284 (2001) 288–295.
[11] E.B. Intyushin, V.A. Novikov, Thin Solid Films 516 (2008) 4194–4200.
[12] D. Tatar, M.L. Öveçoğlu, G. Özen, B. Erim, J. Eur. Ceram. Soc. 29 (2008) 329–335.
[13] B. Öz, I. Kabalcı, M.L. Öveçoğlu, G. Özen, J. Eur. Ceram. Soc. 27 (2007) 3239–3251.
[14] M.L. Öveçoğlu, I. Kabalcı, G. Özen, B. Öz, J. Eur. Ceram. Soc. 27 (2006) 1801–1804.
[15] A.P. Mirgorodsky, T. Merle-Mejean, J.C. Champarnaud, P. Thomas, B. Frit, J. Phys. Chem. Solids 61 (2000) 501–509.
[16] J.C. Champarnaud-Mesjard, S. Blanchandin, P. Thomas, A. Mirgorodsky, T. Merle-Méjean, B. Frit, J. Phys. Chem. Solids 61 (1999) 1499–1507.
[17] V.O. Sokolov, V.G. Plotnichenko, E.M. Dianov, J. Inorg. Mater. 43 (2006) 194–213.
[18] S. Zhao, B. Chen, L. Wen, L. Hu, J. Mater. Chem. Phys. 99 (2005) 210–213.
[19] V.V. Safonov, Russ. J. Inorg. Chem. 53 (2008) 509–511.
[20] A.K. Yakhkind, J. Am. Ceram. Soc. 49 (1966) 670–675.
[21] V. Kozhukharov, M. Marinov, G. Grigorova, J. Non-Cryst. Solids 28 (1978) 429–430.
[22] G. Upender, S. Bharadwaj, A.M. Awasthi, V.C. Mouli, Mater. Chem. Phys. 118 (2009) 298–302.
[23] M. Çelikbilek, A.E. Ersundu, N. Solak, S. Aydın, in: 112th Materials Science & Technology 2010 Conference and Exhibition of the American Ceramic Society, Houston, Texas, USA, October 17–21, 2010.
[24] S.K.J. Al-Ani, C.A. Hogarth, R.A. El-Malawany, J. Mater. Sci. 20 (1985) 661–667.
[25] R. El-Mallawany, I.A. Ahmed, J. Mater. Sci. 43 (2008) 5131–5138.
[26] A.A. Cabral Jr., C. Fredericci, E.D. Zanotto, J. Non-Cryst. Solids 219 (1997) 182–186.
[27] D. Tatar, G. Ozen, F.B. Erim, J. Raman Spectrosc. 41 (2010) 797–807.
[28] G. Upender, V.G. Sathe, V.C. Mouli, Physica B 405 (2010) 1269–1273.
[29] E. Salje, K. Viswanathan, Acta Crystallogr. 31 (1975) 356–359.
[30] Powder Diffraction File, Card No. 42-1365, 1992 Database Edition, Joint Committee on Powder Diffraction Standards (JCPDS), Swathmore, PA, USA.
[31] Powder Diffraction File, Card No. 43-1035, 1992 Database Edition, Joint Committee on Powder Diffraction Standards (JCPDS), Swathmore, PA, USA.